Journal of Materials Chemistry A

ROYAL SOCIETY OF CHEMISTRY

PAPER

View Article Online
View Journal | View Issue

Check for updates

Cite this: *J. Mater. Chem. A*, 2020, **8**, 1887

Hollow spherical SiO_2 micro-container encapsulation of LiCl for high-performance simultaneous heat reallocation and seawater desalination†

Kaijie Yang,[a] Yusuf Shi,[a] Mengchun Wu,[a] Wenbin Wang,[a] Yong Jin,[a] Renyuan Li,[a] Muhammad Wakil Shahzad,[b] Kim Choon Ng[a] and Peng Wang *[ac]

Received 24th October 2019
Accepted 6th December 2019

DOI: 10.1039/c9ta11721k

rsc.li/materials-a

Energy & fresh water have both become scarce resources in the modern era of human society. Sorption-based technology is environmentally friendly and energy-efficient and can be driven by low-grade energy to transfer energy and produce fresh water. Here, we report a solid sorbent fabricated by encapsulating a hygroscopic salt, lithium chloride (LiCl), inside micro-sized hollow-structured SiO_2. This composite sorbent (LiCl@HS) exhibits 6 times faster water vapor sorption kinetics than pure LiCl and a water vapor sorption capacity of 1.7 kg kg^{-1} at a relative humidity (RH) of 50%, which is the highest ever reported for any solid sorbent in the literature. The low regeneration temperature (<80 °C) and good cycling stability ensure the feasibility of the composite sorbent for use in practical applications. The thermodynamic calculations reveal that the sorbent is able to continuously supply 20 °C temperature lift with a maximum coefficient of performance (COP) for cooling of 0.97 and COP for heating of 1.89 while simultaneously producing 9.05 kg potable water per kilogram sorbent daily using seawater as the source water and solar energy as the sole energy source. A homemade system is developed and its practical performance in providing seasonally switchable heating and cooling along with clean water production from source water with an impaired quality is successfully verified, indicating its great potential.

1. Introduction

Building energy consumption, including space cooling and heating, water heating, lighting, cooking, *etc.*, very significant nowadays.[1–4] In the U.S. and E.U., building energy consumption currently accounts for over 40% of total primary energy consumption, out of which 45% is consumed by air conditioning for space cooling and heating.[3–7] The energy demand for space cooling and heating is still on a rapid rise due to the fast population growth, improved standard of living, fast industrialization of developing countries, and global warming.[8,9] It has been estimated that the energy demand for air conditioning will increase rapidly from close to 300 terawatt hours (TW h) in 2000 to about 4000 TW h in 2050 and more than 10 000 TW h in 2100.[10] The International Energy Agency (IEA) has predicted that India's cooling-related energy demand will soar from 90 TW h in 2016 to 1350 TW h in 2050, a 15-fold increase.[11] Thus, it is not an overstatement that the global air conditioning need is becoming one of the major threats to energy security and would further increase global carbon dioxide emissions.[1,12,13]

At the same time, two-thirds of the global population is facing water scarcity to varying extents.[14,15] Due to the inextricable connection between water and energy, water is another factor contributing to the global energy crisis, meaning that there is no effective solution that can solve either the water or energy problem without considering the other.[16,17] Fresh water production, especially *via* seawater desalination, consumes a huge amount of electricity. In Arab countries, for example, more than 15% of the total national electricity is consumed by the fresh water production industry.[18–21]

Adsorptive heat transfer[1,22–24] and adsorptive clean water production,[25–31] which are both powered by low-grade heat energy from sunlight or waste heat, have been separately developed in the last few decades. In the case of water being used as the working fluid in adsorptive heat transfer, the two separate systems can be combined to produce cooling and heating energy and at the same time to produce clean water. The properties of the sorbents are the key parameters for efficiency in heat transfer and clean water production. An ideal

[a]*Water Desalination and Reuse Center, Division of Biological and Environmental Science and Engineering, King Abdullah University of Science and Technology, Thuwal 23955-6900, Saudi Arabia. E-mail: peng.wang@kaust.edu.sa*

[b]*Department of Mechanical and Construction Engineering, Northumbria University, Newcastle Upon Tyne NE18ST, UK*

[c]*Department of Civil and Environmental Engineering, The Hong Kong Polytechnic University, Hung Hom, Kowloon, Hong Kong*

† Electronic supplementary information (ESI) available. See DOI: 10.1039/c9ta11721k

sorbent for the combined system should possess a large water sorption capacity, fast sorption and desorption kinetics, easy regeneration and cycling performance stability.

Up to now, silica gel has had a limited water sorption capacity, zeolites have required a high regeneration temperature, and fabrication of metal–organic frameworks (MOFs) has been very costly. Liquid desiccants based on hygroscopic salts, such as lithium chloride (LiCl), calcium chloride ($CaCl_2$), and lithium bromide (LiBr), indeed possess good water vapor sorption capacity and reasonable desorption temperature, but they suffer from difficulty in handling and high mobility due to their liquid nature after deliquescence.[1,3,5,13,14,23] Recently, the concept of a composite sorbent which holds a liquid desiccant in a solid matrix has emerged as a possible solution. Matrixes, such as natural rock, porous fibers, and silica gel, have been reported as liquid desiccants.[3,14]

In the search for a more effective sorbent, our attention is drawn to hollow structures that have a large internal space.[32–35] The hollow structure can serve as a semipermeable container which keeps the liquid sorbent inside and at the same time allows free passage of water vapor. In this study, we developed a micro-sized hollow SiO_2 sphere (HS) with a porous wall, which allowed LiCl to be impregnated easily inside the hollow chamber. With a rationally controlled LiCl loading amount, the large hollow space of the hollow micro container acted as the water storage site and the composite sorbent produced a record-high water vapor sorption capacity among all of the solid sorbents in the literature. In addition, the encapsulation strategy enhanced the surface area of the sorbent accessible to water vapor, leading to much faster (*e.g.*, 6 times faster) sorption kinetics relative to pure LiCl. The sorbed water could be released at a desorption temperature of 70 °C and there was no performance degradation after 10 sorption–desorption cycles. The excellent water sorption–desorption performance of the sorbent led to an excellent heat transfer and water production performance, producing a COP for cooling of 0.97 and COP for heating of 1.89. Based on the experimental results, the thermodynamics of the processes was calculated to reveal its detailed heat transfer and water production capability. A homemade setup was used to successfully validate its viability in providing seasonally flexible cooling and heating along with simultaneous seawater desalination to produce clean drinking water for a household. It is envisioned that such a system underpinned by an effective sorbent can make significant contributions to address the ongoing global clean energy shortage and fresh water scarcity.

2. Results and discussion

2.1. Materials design and fabrication

The fabrication procedure of the hollow silica spheres used in this work is illustrated in Fig. 1. Amphiphilic polyethylene glycol (PEG) modified hyper-branched polyethoxysiloxane (PEOS), denoted as PEG–PEOS, was first synthesized as a silica source following a literature method.[36] In PEG–PEOS, the PEOS head part is hydrophobic while the PEG tail is hydrophilic. When it is mixed into a mixture of deionized water and trimethylbenzene (TMB), it facilitates the formation of a water-in-oil emulsion where PEG–PEOS assembles at the water/oil interface due to its amphiphilic structure (process I). The addition of $NH_3 \cdot H_2O$ causes PEOS to be converted to a silica shell surrounding the water droplets. Drying then removes the water and produces hollow SiO_2 structures (HS) (process II). In this step, the water droplet acts as a template and the size of the water droplets in the TMB solvent is determined by the stirring strength and the affinity between water and TMB.

Lithium chloride (LiCl) was loaded into HS by the wet impregnation method followed by drying in air at 100 °C (process III). The loading amount was controlled by the concentration of the LiCl aqueous solution. The obtained final composite sorbents are denoted as LiCl@HS-*X*, in which *X* represents the amount (mg) of LiCl in each milliliter of void space inside HS. For example, HS-500 indicates that the concentration of the LiCl precursor solution is 500 mg cm^{-3}. In other words, after impregnation, 1 cm^3 of void space of the silica hollow sphere contains 500 mg LiCl. The void interior of HS serves as both the salt container and storage space of the sorbed water, while the porous shell acts as a water vapor exchange window. Compared with the soft composite sorbents that are easily deformed during sorption, this hard SiO_2 framework can avoid the shortcoming of deformation.[12]

Fig. 2A–C display the SEM images of the HS. As can be seen, the diameters of these spheres were 60–80 μm with an average diameter of around 100 μm (Fig. S1†). The large HS particle size is advantageous, as it makes direct HS packing into a sorption bed possible while preserving sufficient inter-particle channels for moist air transport (Fig. S2†). Fig. 2B reveals the rough and porous external surface of a silica sphere and Fig. 2C indicates that the silica shell is composed of tightly assembled silica nanoparticles. The hollow interior of HS can be directly viewed in some broken particles (Fig. S3†). The thickness and pore size of the shell are estimated to be approximately 70 nm (Fig. S3†) and 10–100 nm (Fig. S4A and B†), respectively. The porous shell ensures successful LiCl impregnation during sorbent

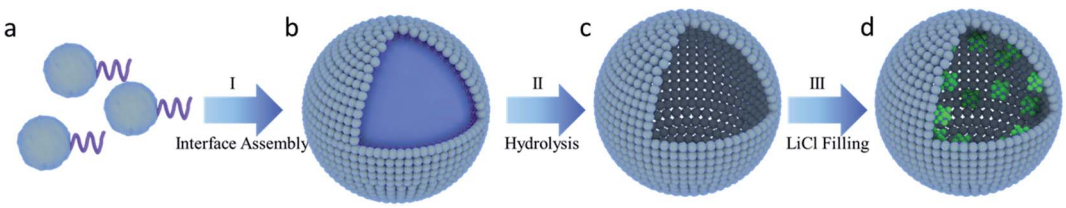

Fig. 1 Schematic illustration of hollow structure fabrication and LiCl impregnation.

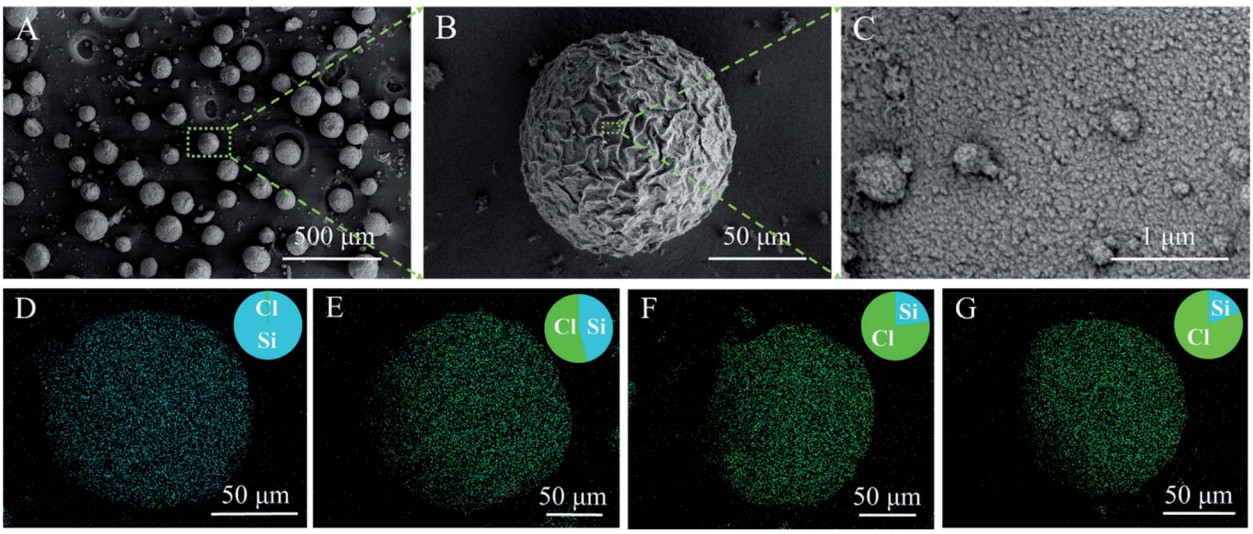

Fig. 2 Structural characterization of HS. (A) Large scale SEM observation of HS spheres, (B) external surface morphology of a single HS particle, (C) a close-up image of the surface structure of HS, and EDS images of (D) pure HS, (E) HS-200, (F) HS-500, and (G) HS-700. The insets in (D)–(G) are the Cl : Si mass ratios measured by EDS mapping.

fabrication and water vapor passage in and out during water vapor uptake and release operations.

Both XRD investigation (Fig. S5†) and SEM observation (Fig. S6 and S7†) confirm the presence of LiCl crystals inside HS. The specific surface area of LiCl@HS decreased with an increase in the LiCl loading amount (Fig. S4C†). SEM observation revealed that the LiCl@HS presented a relatively clear surface (Fig. S6†). In some broken silica hollow spheres, the presence of a LiCl crystal inside the hollow void could be directly observed (Fig. S7†). All these results indicate that LiCl crystals were successfully encapsulated inside the silica hollow spheres.

The LiCl loading percentages were determined to be 39.5% for HS-200, 67.6% for HS-500 and 72.7% for HS-700 (Fig. S8†). Fig. 2D–G present the EDS maps of HS, which show the mass ratio of LiCl in HS-200, HS-500 and HS-700 to be 39.6%, 65.2%, and 70.4%, respectively. These results are in good agreement with those obtained by the weighing method.

2.2. Water vapor sorption evaluation

Water vapor sorption behaviors of the pristine HS and LiCl@HS are shown in Fig. 3. Pure HS had a very small water sorption capacity of 0.03 kg kg^{-1} at 25 °C and 20% relative humidity (RH). In sharp contrast, HS-200, HS-500, and HS-700 exhibited water vapor sorption capacities of 0.60, 0.98 and 1.15 kg kg^{-1} at 20% RH, respectively. These results clearly demonstrate that the sorption capacity of LiCl@HS is mainly due to the encapsulated LiCl salt, and the silica container itself contributed negligibly to the overall water sorption capacity of the composite LiCl@HS. The kinetics of LiCl@HS at 50% and 80% RH are presented in Fig. S9.† Based on the water sorption capacity of pure LiCl of 1.48 kg kg^{-1} at 20% RH (Fig. S10†), the theoretical water sorption capacities of LiCl@HS are estimated to be 0.59, 0.96 and 1.04 kg kg^{-1} for HS-200, HS-500 and HS-700, respectively, all of which are close to the measured values (Fig. 3A).

As LiCl salt sorbs water, it gets dissolved in the sorbed water and turns into a liquid form, a phenomenon commonly known as deliquescence, which causes difficulties in practical operation.[3,37] In this work, LiCl is rationally encapsulated inside the silica hollow sphere as a micro-container. The results show that the micro-container had no adverse effects on the water sorption capacity of the impregnated LiCl while it restrained the deliquescent liquid inside the solid container, which offers substantial merits in practical applications. From a kinetics point of view, pure LiCl salt suffers from very slow vapor sorption kinetics, needing ~600 min to reach its sorption equilibrium (Fig. S10†). During the early stage of deliquescence, a water film would form (Fig. S11†) and any further vapor sorption by the salt crystal would have to be *via* slow molecular diffusion through the water film, leading to overall sluggish sorption kinetics.[37] In comparison, LiCl@HS possessed much faster sorption kinetics (Fig. 3). For example, HS-500 took ~100 min to reach its sorption equilibrium under the same conditions, which is 6 times faster than that for pure LiCl (Fig. 3B).

These results convincingly demonstrate that LiCl@HS designed in this work delivers the promised enhanced vapor sorption kinetics along with an uncompromising sorption capacity. In this work, the amount of LiCl inside the micro-container is determined and controlled so that the final liquefied LiCl stays inside the container as small droplets with a high surface area, that is, the volume of the LiCl solution is controlled to always be smaller than the void space of the container. Furthermore, the inter-particle void space among the packed HS spheres acts as the vapor mass transport highway. Thus, our design of the encapsulated and well-separated LiCl droplets minimizes the molecular diffusion limitation otherwise observed in the conventional bulk LiCl based systems and, at the same time, the mass transfer highway provides each

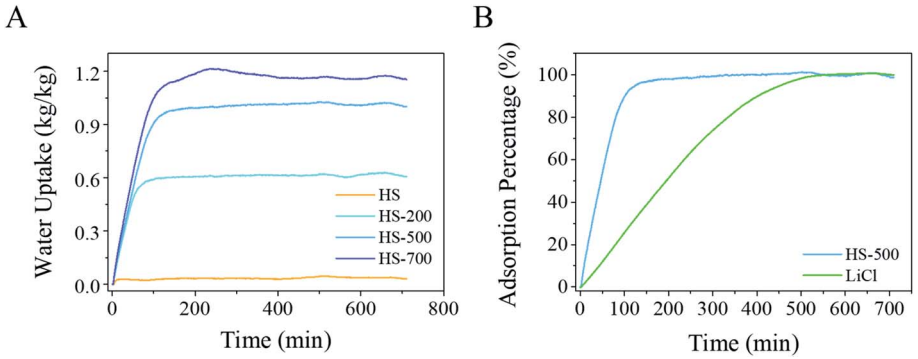

Fig. 3 Water vapor sorption. (A) Sorption kinetics at 20% RH and (B) kinetics comparison of HS-500 and LiCl particles.

sorption unit with fast access to water vapor, synergistically leading to much-improved vapor sorption kinetics and uncompromised sorption capacity.

Water vapor sorption isotherms of the HS and LiC@HS samples were measured at 25 °C (Fig. 4A and S12†) and all the samples exhibited type II isotherms, suggesting their highly hydrophilic properties.[3] At 10% RH, the sorption capacities were 0.24, 0.35 and 0.54 kg kg^{-1} for HS-200, HS-500, and HS-700, respectively, indicating a strong affinity to water vapor of the composite material under dry conditions (Fig. 4A).

For all these samples, the sorption capacities gradually increased with an increase in the RH, which is quite similar to that of pure LiCl salt as reported in numerous studies.[3,38] Compared with existing porous materials (*e.g.*, MOF,[13,26] zeolite,[3] and silica gel[3]) and composite sorbents (*e.g.*, AFC–LiCl[39] and SG–LiCl[14]) that have been intensively investigated for water vapor sorption, LiCl@HS in this work exhibited considerably higher capacity under comparable conditions (Fig. 4B).

It should be noted that these micro-containers have their own limitation on maximal sorption capacity, beyond which leakage of the liquefied salt and aggregation of sorbents will occur. For example, HS-200 has 200 mg LiCl per 1 cm^3 of internal space and 200 mg LiCl can adsorb a maximum of 1 g water under 85% RH according to the water absorption isotherms (Fig. S13†). Since the LiCl content has little effect on its solution density, the volume of the liquefied LiCl inside HS-200 can barely fill up the entire internal void space of HS (around 1 cm^3) at its sorption maximum. Therefore, when HS-

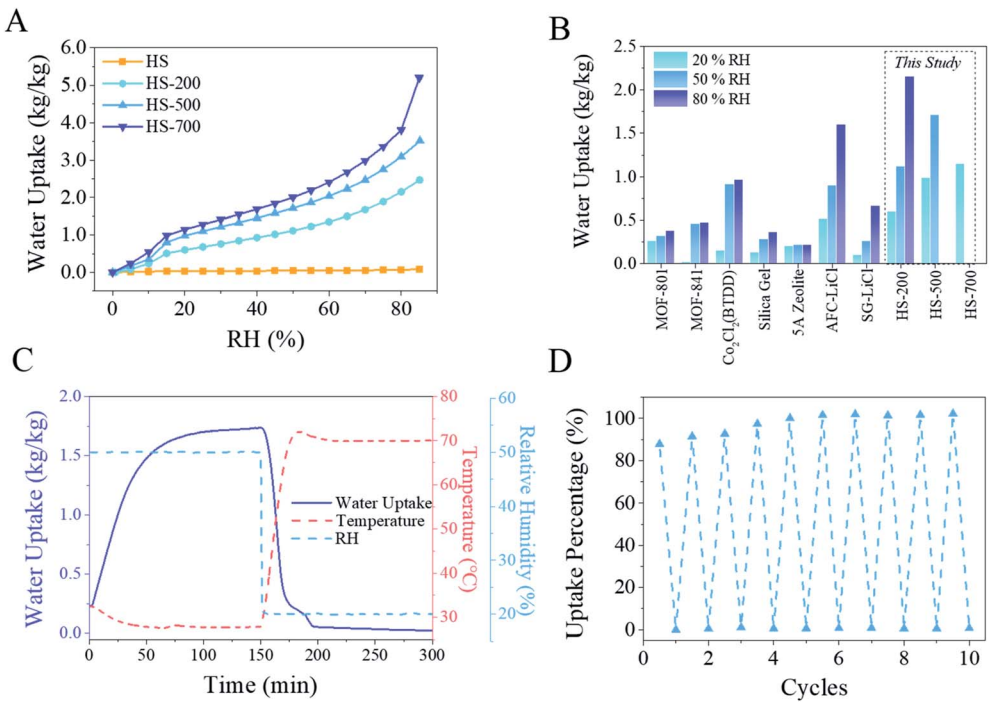

Fig. 4 Sorption capacity and recycling performance. (A) Sorption isotherms of sorbents at 25 °C, (B) sorption capacity comparison, (C) sorption and desorption performance of HS-500, and (D) cycling evaluation of HS-500 (sorption conditions: 50% RH at 30 °C; desorption conditions: 20% RH at 70 °C).

200 is exposed to air with a RH < 85%, the volume of the LiCl solution would be smaller than the available void space of the hollow spheres and thus it will stay inside. Similarly, with an RH > 85%, liquefied LiCl will overflow and leak out of the hollow spheres, and the LiCl which flowed out would block the inter-particle pore space and lead to particle agglomeration, deteriorating the system's performance. As a result, the working RH range for HS-200 is ≤ 85%. Likewise, the working RH ranges for HS-500 and HS-700 are similarly estimated to be ≤ 50% and ≤ 20% RH, respectively. Our results confirm that when HS-200, HS-500, and HS-700 were exposed to air for 6 hours with an RH of 85%, 50%, and 20%, respectively, all these samples maintained their loosely packed dry powder form after reaching their sorption limits (Fig. S14†). It is imperative that HS@LiCl maintain a dry state as an agglomerated state of the sorbents defeats its design purpose (Fig. S15†).

2.3. Heat transfer evaluation with seawater

Owing to the superior water sorption performance of LiCl@HS, its heat transfer and water production ability were investigated, using seawater as the source water. During the evaluation, the working temperature of the LiCl@HS sorbent was set at 30 °C as in most of the literature studies and also because it is close to the conditions in practical applications.

When the temperature of aerated seawater rises from 0 °C to 30 °C, its saturated vapor pressure increases from 0.60 kPa to 4.16 kPa (Fig. S16†). The corresponding RH around the sorbent (at a 30 °C working temperature), generated by the aerated seawater, increases from 14.1% (0 °C seawater) to 98.0% (30 °C seawater) (Fig. S17†). Based on the previous discussion on the working RH ranges of LiCl@HS, HS-200, HS-500, and HS-700 are deemed suitable to work in temperature lift ranges of 0–12 °C, 12–25 °C, and 25–30 °C, respectively. Temperature lift is the difference between the temperature of sorbents and seawater and typically represents the temperature difference between the indoors and the outdoors in practical applications. A temperature lift of 20 °C is required for commercially viable air conditioning applications, and HS-500 is thus the most suitable sorbent among all three.[2,13] It is for this reason that only HS-500 was used for the subsequent performance evaluation unless otherwise specified.

The enthalpy (ΔH_{ads}) of water sorption for HS-500 is determined from the water vapor sorption isotherms (Fig. S18 and S19†) according to the Clausius–Clapeyron equation. As can be seen, ΔH_{ads} gradually decreased from 47 kJ mol^{-1} to 43 kJ mol^{-1} as water sorption continued. The average enthalpy of water sorption was calculated to be 44 kJ mol^{-1} (2430 kJ kg^{-1}), close to the heat of vaporization of water at 30 °C (Fig. S20†),[40] indicating that hydrogen bonding between water molecules is the dominant force during sorption.[5,13] The weak interaction between water and the sorbent leads to energy-efficient regeneration of HS-500. Once the temperature and RH were changed to 70 °C and 20%, the sorbed water was quickly released and it

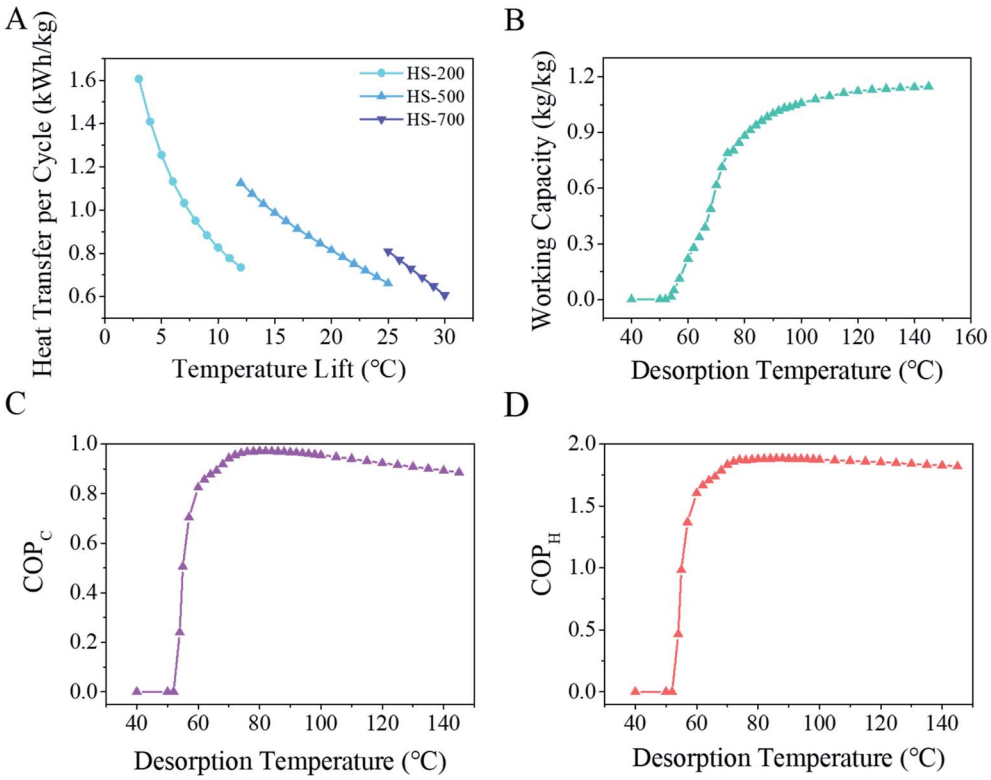

Fig. 5 Thermodynamic performance of HS-500. (A) Heat energy transfer per cycle as a function of the temperature lift, (B) working capacity at a 20 °C temperature lift, (C) COP for cooling with a 20 °C temperature lift (10 °C chiller and 30 °C ambient), and (D) COP for heating with a 20 °C temperature lift (30 °C heater and 10 °C ambient).

reached equilibrium in 40 min (Fig. 4C). Fig. 4D presents its water sorption and release cycling performance and, as revealed, there was no discernible performance degradation after 10 cycles.

The psychometric chart in Fig. S21† presents the basic physical and thermodynamic properties of water desorption within the vapor sorption-based heat reallocation and water production system. Under heating, the temperature of the sorbent and ambient air is increased from 25 to 70 °C (Fig. S21, I–II†) and water vapor is released from the sorbent which in turn increases the air humidity (Fig. S21, II–III†). The humid air flows into and is subsequently cooled down in the condenser to its dew point (Fig. S21, III–IV†). In the last step, the saturated wet air is further cooled to produce condensed water (Fig. S21, IV–I†). Such a closed cycle is more energy efficient than open ones.[12]

Sorption isotherms at different temperatures allow for the calculation of characteristic curves.[2] With the isotherms, two dependent variables, temperature and pressure, can be converted into a single variable, Gibbs free energy (Fig. S22†), with which isotherms at any given temperature, heat transfer (Fig. S23†) of the system, working capacity of the sorbent, and coefficient of performance (COP) for heat transfer can all be computed sequentially. Fig. 5A presents the calculated heat transfer abilities based on the temperature lift. As can be seen, with HS-500, a heat pump requiring a 20 °C temperature lift can be achieved with a heat transfer capacity of 0.81 kW h per kg per cycle for HS-500, which is at least 0.2 kW h kg^{-1} higher than that of any known solid sorbent.[2,5,13] The working capacity increased with the increasing desorption temperature as expected (Fig. 5B) because a higher temperature can result in more water being extracted from the sorbent during the sorbent regeneration step. A maximum COP_C of 0.97 and COP_H of 1.88 were achieved when the desorption temperature was set at 80 °C (Fig. 5C and D) at which HS-500 had a working capacity of 0.88 kg kg^{-1}, the highest working capacity for a solid sorbent to the best of our knowledge.[2,5,13]

This means about 2.1 MJ heat energy can be transferred and 0.88 kg fresh water can be produced by one kilogram of the sorbent in each sorption–desorption cycle. Such high performance should be ascribed to the super sorption capacity and easy regeneration at relatively low temperatures for this material. This optimized desorption temperature of 80 °C can be readily achieved using commercial solar collectors which can generate 60–100 °C hot water.[12] As each sorption–desorption cycle takes around 140 min (Fig. 4C), one kilogram of HS-500 is able to transfer 22 MJ heat energy from the indoors to the outdoors and simultaneously produce 9.05 kg of fresh water from seawater in one day.

2.4. Laboratory verification of combined heat transfer and desalination

The LiCl@HS sorbent was further utilized for combined heat transfer and seawater desalination. As a matter of fact, we believe that the integration of heat transfer and desalination of seawater, or other suitable water sources with impaired quality, is a niche application of our material. The integrated system can achieve simultaneous house cooling and clean water production from seawater during hot days or simultaneous house heating and clean water production from seawater on cold days, using solar energy as the sole energy source (Fig. 6A).

In hot weather (Fig. 6A, left part), the evaporation of seawater, driven by water sorption of LiCl@HS, produces the desired cooling power for indoor cooling. Regeneration of the sorbent is achieved using solar heat to complete the cycle and produce fresh water simultaneously. The sorption cycle and desorption cycle are designed to be separate but, with easily switchable sorbent beds, the system can work continuously without interruption. On the other hand, on cold days (Fig. 6A, right part), the sorption heat, generated during water sorption onto the LiCl@HS sorbent, is utilized for indoor heating. At the same time, solar generated water vapor from the saturated sorbents can also be used to generate additional heat during the condensation process to warm the room. Clean water is produced at the same time from seawater. The seasonal switch of these two operation modes (*i.e.*, cooling and heating) can be achieved by exchanging the corresponding components between the indoors and outdoors. For hot climate and cold climate regions, the system can be permanently set to the cooling or heating mode.

To test the practical viability of our system design, a laboratory setup was built to evaluate its cooling, heating and desalination performance, using seawater as the source water and simulated solar energy as the energy source (Fig. S24–S26†). Seawater was taken directly from the Red Sea along the campus of the KAUST, Thuwal, Saudi Arabia (Fig. S27†). For cooling performance evaluation, the blowing air flow rate was set at 500 ml min^{-1} and the temperature of the sorbents was maintained at 30 °C. Although heat exchange was always present between the seawater and incoming hot air, the seawater temperature gradually decreased from 30 °C to 8 °C (Fig. 6B). The saturated vapor pressure of the seawater at 8 °C is 1.05 kPa (Fig. S9†) and, under these conditions, HS-500 still possesses a sorption capacity of 1 kg kg^{-1}, which can well satisfy the cooling performance (Fig. S28†). Theoretically, HS-500 is able to cool the seawater down to 0 °C because, under the vapor pressure generated by 0 °C seawater (0.60 kPa), HS-500 can still sorb vapor and thus transfer heat from seawater. However, with the heat exchange between the inlet hot air and cool seawater, the lowest seawater temperature measured in our lab was 8 °C when HS-500 was used as the sorbent.

For heating evaluation, the seawater was maintained at 10 °C for cold weather simulation. As sorption continued, the sorbent temperature increased gradually from 10 °C to 32 °C (Fig. 6C). The infrared photo shown in Fig. 6E visually revealed the temperature of the cooling seawater and heating sorbent. With the vapor pressure of 10 °C seawater at 1.20 kPa, 1 g HS-500 sorbed 1.3 g water. After desorption at 80 °C, 1 g vapor was produced which, when condensed (Fig. 6F), released 2.43 kJ heat energy to heat the room.

It is worth mentioning that, in the laboratory system evaluation, the condenser temperature was maintained at 20 °C, a little lower than room temperature (25 °C), so condensed

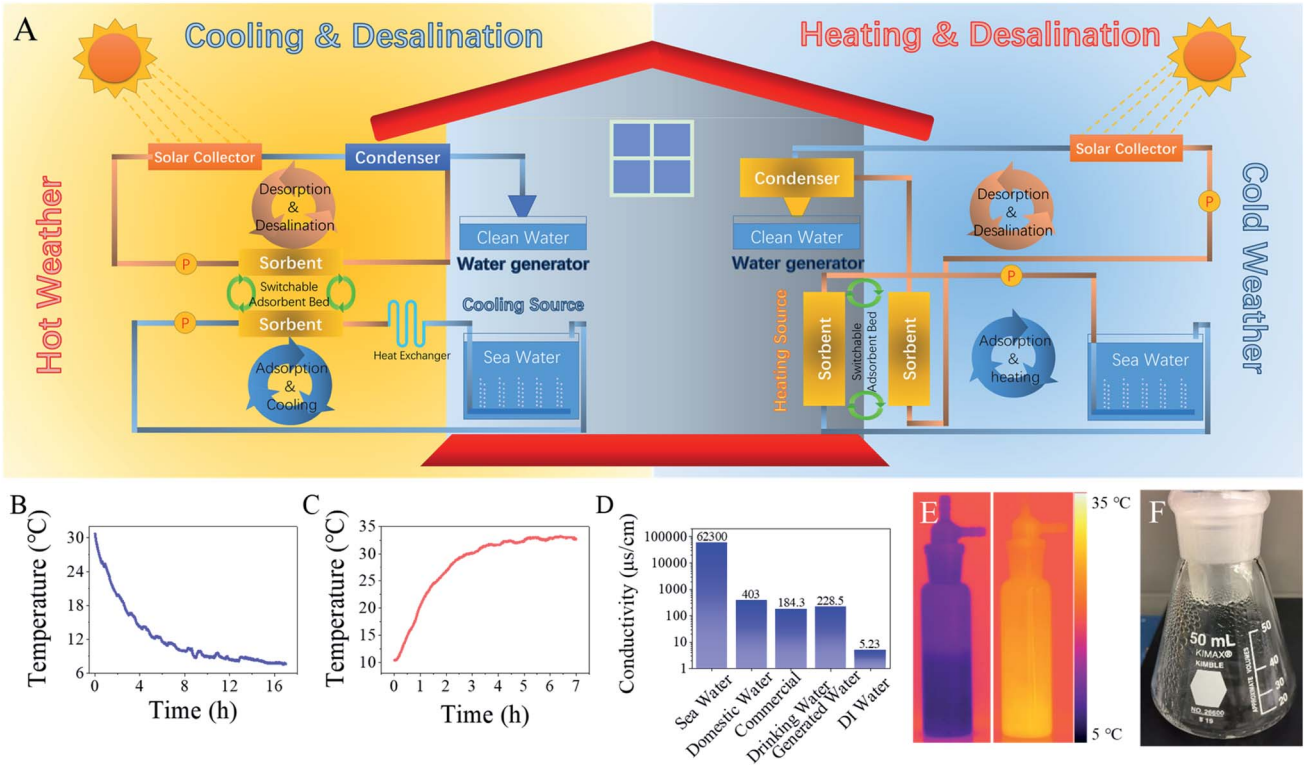

Fig. 6 (A) Conceptual design of heat transfer & desalination for switchable household heating and cooling, (B) temperature curve of cooling seawater and (C) temperature curve of heating sorbents as a function of time, (D) comparison of the conductivity of produced water (PW), seawater (SW), domestic water (DW), commercial drinking water (CDW) and deionized water (DIW), (E) infrared photo of cooling seawater and heating sorbents, and (F) photo of the collected condensed water inside the condenser.

water can be collected within the condenser instead of in the pipeline. The heat released during vapor condensation was directly released to the laboratory room and was hard to measure accurately. Also, since seawater was used as the source water, the system is not suitable for areas with ambient temperature below the seawater freezing point (around −2 °C).

In this composite system, seawater desalination is combined with cooling/heating applications and fresh water is produced during sorbent regeneration. To evaluate its prospects in practical applications, in our homemade system, the temperature of the airflow and sorbents was maintained at 80 °C (Fig. S27†) to simulate the temperature that a solar collector can generate. Under heating, the saturated sorbents began to release heated water vapor, which was cooled down and condensed inside the condenser (Fig. 6F). Measurement of the conductivity (Fig. 6D) and ion concentrations (Fig. S29†) of the produced water (PW) shows that the produced condensate water was in compliance with WHO drinking water standards,[41] indicating the excellent desalination ability of this sorption-based system.[41]

3. Conclusions

In this work, a solid composite sorbent with LiCl encapsulated inside hollow micro-sized SiO_2 spheres was designed and synthesized. This composite sorbent delivered significantly enhanced water vapor sorption kinetics and produced a record-high water vapor sorption capacity among solid sorbents in the literature. With an achievable temperature lift at 20 °C in a heat reallocation system, a maximum COP for cooling of 0.97 and COP for heating of 1.89 can be achieved using this sorbent. The heat reallocation, when combined with seawater desalination, could produce 9.05 kg potable water per kilogram sorbent daily using seawater as the source water and solar energy as the sole energy source.

4. Materials and methods

4.1. Amphiphilic silica precursor synthesis

The precursor was synthesized as follows: 1 mol tetraethoxysilane was mixed with 1 mol acetic anhydride and 0.003 mol tetraethyl orthotitanate for catalysis. The mixture was allowed to react under magnetic stirring (700 rpm) at 135 °C until no ethyl acetate could be distilled out. Then, 65 ml PEG-350 was added and further reacted for 4 h at 135 °C. Afterward, the unreacted volatile fraction was distilled off by vacuum drying. The resultant transparent yellow liquid was the desired amphiphilic silica precursor.

4.2. Hollow structure assembly and LiCl filling

Micro hollow SiO_2 (HS) was self-assembled at the water–oil interface. Firstly, 10 g synthesized precursor was dispersed in 170 ml water under strong stirring to form a homogeneous

solution. Then 160 g trimethylbenzene (TMB) was added. After mixing under strong magnetic stirring (700 rpm), 20 ml $NH_3 \cdot H_2O$ was gradually added. To avoid structural damage during self-assembly, stirring was stopped after 5 min and hydrolysis was carried out for 12 h to convert the silica precursor completely to solid SiO_2. The obtained particles were separated by filtration and washed with alcohol and acetone, followed by drying at 60 °C.

LiCl was filled by a vacuum & pressure release cycle. Fabricated HS was first immersed in a LiCl solution and then placed in a vacuum chamber. The LiCl solutions were prepared by dissolving 20 g, 50 g, and 70 g LiCl salt into 100 ml deionized water, respectively. The obtained sorbents were named HS-200, HS-500, and HS-700, respectively. The obtained materials were dried at 100 °C and stored properly before use.

4.3. Structural characterization and water vapor sorption evaluation

The structure of the sorbents was characterized by SEM, EDX, XRD, and BET analysis. And their water sorption–desorption capacity was evaluated with kinetics, isotherms and cycling performance. The concentration of ions in water was measured by ICP-MS. Water vapor sorption kinetics was evaluated by STA. During the evaluation, the sorbent temperature was set at 25 °C, and the surrounding RH was controlled by a humidity generator. Evaluation stopped once the sorbents' weight was unchanged. Vapor sorption isotherms were obtained using an IGAsorp. The RH range was set from 0% to 85% at an interval of 5%. A homemade system was assembled using laboratory devices (detailed information can be found in the ESI†). The temperatures of the sorbents and seawater were measured using a temperature sensor. Their infrared photos were obtained using an infrared camera. Condensed water was collected using a conical flask attached to the end of the condenser.

4.4. Thermodynamic parameter calculation

Thermodynamic calculations were employed to evaluate the capacity of the sorbents in the heat pump. The calculation process of sorption enthalpy (ΔH_{ads}), sorption potential (A), heat transfer (HT), evaporation heat (Q_{evp}), sorption heat ($Q_{sorption}$), condensation heat (Q_{cond}), regeneration energy (Q_{regen}), coefficient of performance for cooling (COP_C) and coefficient of performance for heating (COP_H) is presented in the ESI.†

Conflicts of interest

There are no conflicts to declare.

References

1 D. Lenzen, P. Bendix, H. Reinsch, D. Fröhlich, H. Kummer, M. Möllers, P. P. C. Hügenell, R. Gläser, S. Henninger and N. Stock, *Adv. Mater.*, 2018, **30**, 1705869.
2 M. F. de Lange, K. J. F. M. Verouden, T. J. H. Vlugt, J. Gascon and F. Kapteijn, *Chem. Rev.*, 2015, **115**, 12205.
3 X. Zheng, T. S. Ge and R. Z. Wang, *Energy*, 2014, **74**, 280.
4 X. Cao, X. Dai and J. Liu, *Energy Build.*, 2016, **128**, 198.
5 A. J. Rieth, A. M. Wright, S. Rao, H. Kim, A. D. LaPotin, E. N. Wang and M. Dincă, *J. Am. Chem. Soc.*, 2018, **140**, 17591.
6 J. Mandal, Y. Fu, A. C. Overvig, M. Jia, K. Sun, N. N. Shi, H. Zhou, X. Xiao, N. Yu and Y. Yang, *Science*, 2018, **362**, 315.
7 J. M. S. Dias and V. A. F. Costa, *Renew. Sustain. Energy Rev.*, 2018, **98**, 317.
8 A. Alahmer, S. Ajib and X. Wang, *Renew. Sustain. Energy Rev.*, 2019, **99**, 138.
9 L. Yang and J. Xia, *Procedia Eng.*, 2015, **121**, 1887.
10 M. Isaac and D. P. van Vuuren, *Energy Policy*, 2009, **37**, 507.
11 K. Ito, Y. Yamashita, A. Yanagisawa, Z. Lu, S. Endo, R. Eto, T. Kato, K. Koyama, T. Murakami, T. Ohira, K. Taguchi, K. Shimogori, A. Suzuki, A. Kuroki, T. Tagami, K. Komatsu, Y. Kobayashi, T. Morikawa, A. Sagawa, Y. Nagatomi, Y. Kawakami, Y. Shibata, K. Sichao and R. Casauon, *Outlook 2018 - Prospects and Challenges until 2050 - Energy, Environment and Economy*, ed. C. Onda and A. Nakata, The Institute of Energy Economics, Japan 2018.
12 H. Li, Y. J. Dai, Y. Li, D. La and R. Z. Wang, *Appl. Therm. Eng.*, 2011, **31**, 3677.
13 A. J. Rieth, S. Yang, E. N. Wang and M. Dincă, *ACS Cent. Sci.*, 2017, **3**, 668.
14 Y. Tu, R. Wang, J. Wang and Y. Zhang, *Joule*, 2018, **2**, 1452.
15 M. M. Mekonnen and A. Y. Hoekstra, *Sci. Adv.*, 2016, **2**, e1500323.
16 A. Deshmukh, C. Boo, V. Karanikola, S. Lin, A. P. Straub, T. Tong, D. M. Warsinger and M. Elimelech, *Energy Environ. Sci.*, 2018, **11**, 1177.
17 M. Gao, L. Zhu, C. K. Peh and G. W. Ho, *Energy Environ. Sci.*, 2019, **12**, 841.
18 J. R. Ziolkowska, *Water Resour. Manag.*, 2015, **29**, 1385.
19 M. A. Shannon, P. W. Bohn, M. Elimelech, J. G. Georgiadis, B. J. Mariñas and A. M. Mayes, *Nature*, 2008, **452**, 301.
20 M. Elimelech and W. A. Phillip, *Science*, 2011, **333**, 712.
21 N. V. Jagannathan, A. S. Mohamed and A. Kremer, *Water in the Arab World: Management Perspective and Innovations*, The Word Bank, 2018.
22 C. R. Wade, T. Corrales-Sanchez, T. C. Narayan and M. Dincă, *Energy Environ. Sci.*, 2013, **6**, 2172.
23 A. Krajnc, J. Varlec, M. Mazaj, A. Ristić, N. Z. Logar and G. Mali, *Adv. Energy Mater.*, 2017, **7**, 1601815.
24 A. Permyakova, S. Wang, E. Courbon, F. Nouar, N. Heymans, P. D'Ans, N. Barrier, P. Billemont, G. De Weireld, N. Steunou, M. Frère and C. Serre, *J. Mater. Chem. A*, 2017, **5**, 12889.
25 F. Fathieh, M. J. Kalmutzki, E. A. Kapustin, P. J. Waller, J. Yang and O. M. Yaghi, *Sci. Adv.*, 2018, **4**, t3198.
26 H. Kim, S. Yang, S. R. Rao, S. Narayanan, E. A. Kapustin, H. Furukawa, A. S. Umans, O. M. Yaghi and E. N. Wang, *Science*, 2017, **356**, 430.
27 R. Li, Y. Shi, M. Alsaedi, M. Wu, L. Shi and P. Wang, *Environ. Sci. Technol.*, 2018, **52**, 11367.
28 R. Li, Y. Shi, L. Shi, M. Alsaedi and P. Wang, *Environ. Sci. Technol.*, 2018, **52**, 5398.

29 M. J. Kalmutzki, C. S. Diercks and O. M. Yaghi, *Adv. Mater.*, 2018, **30**, 1704304.
30 F. Zhao, X. Zhou, Y. Liu, Y. Shi, Y. Dai and G. Yu, *Adv. Mater.*, 2019, **31**, 1806446.
31 X. Zhou, Y. Guo, F. Zhao and G. Yu, *Acc. Chem. Res.*, 2019, **52**, 3244.
32 S. Cao, L. Fang, Z. Zhao, Y. Ge, S. Piletsky and A. P. F. Turner, *Adv. Funct. Mater.*, 2013, **23**, 2162.
33 Y. Li and J. Shi, *Adv. Mater.*, 2014, **26**, 3176.
34 P. Ruckdeschel, A. Philipp and M. Retsch, *Adv. Funct. Mater.*, 2017, **27**, 1702256.
35 X. W. D. Lou, L. A. Archer and Z. Yang, *Adv. Mater.*, 2008, **20**, 3987.
36 H. Wang, G. Agrawal, L. Tsarkova, X. Zhu and M. Möller, *Adv. Mater.*, 2013, **25**, 1017.
37 L. J. Mauer and L. S. Taylor, *Annu. Rev. Food Sci. Technol.*, 2010, **1**, 41.
38 X. Zheng, T. S. Ge, Y. Jiang and R. Z. Wang, *Int. J. Refrig.*, 2015, **51**, 24.
39 J. Y. Wang, R. Z. Wang, Y. D. Tu and L. W. Wang, *Energy*, 2018, **165**, 387.
40 J. R. Elliott and C. T. Lira, *Introductory Chemical Engineering Thermodynamics*, Prentice Hall , 2nd edn, 2012.
41 World Health Organization, *Guidelines for drinking-water quality*, 4th edn, 2017.